Catalysis Today 164 (2011) 221–226

Contents lists available at ScienceDirect

Catalysis Today

journal homepage: www.elsevier.com/locate/cattod

Kinetic study of methane CO_2 reforming on Co–Ni/Al_2O_3 and Ce–Co–Ni/Al_2O_3 catalysts☆

Say Yei Foo, Chin Kui Cheng, Tuan-Huy Nguyen, Adesoji A. Adesina*

Reactor Engineering and Technology Group, School of Chemical Engineering, The University of New South Wales, Anzac Parade, Kensington, Sydney, New South Wales 2052, Australia

ARTICLE INFO

Article history:
Received 1 July 2010
Received in revised form 26 October 2010
Accepted 31 October 2010
Available online 3 December 2010

Keywords:
CO_2 reforming of CH_4
Cobalt–nickel catalyst
Cerium promoter
Kinetic analysis

ABSTRACT

The performance of Ce-promoted and undoped 5Co–15Ni/Al_2O_3 catalysts for the dry reforming of CH_4 has been investigated in a fixed-bed reactor. Although addition of Ce (2.5 wt%) significantly reduced carbon deposition by up to 50%, there was neither marked improvement in CH_4 reaction rate (<5% increase) nor a significant change in activation energy. The increased carbon resistance of the Ce-promoted catalyst was attributed to equilibrium between stable multiple oxidation states of the Ce ion during the reaction. TPR–TPO of used catalysts revealed the existence of two types of carbon species-reactive C_α which is easily gasified by H_2 and also participates in redox reactions with cerium oxides, and a relatively non-reactive C_β which is only removed by O_2 and does not participate in the redox cycle. A dual-site Langmuir–Hinshelwood mechanism for the reaction was also proposed.

1. Introduction

Synthesis gas (H_2 and CO) is primarily produced from the catalytic steam reforming of natural gas (mostly methane). With increasing concern on the rise of anthropogenic greenhouse gas emissions, CO_2 (dry) reforming of hydrocarbons has emerged as a viable alternative to steam reforming. Implementation of dry reforming rather than conventional steam reforming is attractive in areas where water is not readily available. Since CO_2 is present in most natural gas fields, reforming may also be carried out without pre-separation of CO_2 from natural gas [1].

Hydrocarbon reforming is conventionally carried out on Ni-based catalyst, which suffers from carbon-induced deactivation. Noble metals such as Ru, Rh, Pt, Pd and Ir are highly active and carbon resistant [2–5], however they are seldom used industrially due to limited availability and high cost. Various methods have therefore been investigated to improve Ni-containing catalysts, including the effect of supports [6,7], bimetallic catalysts [8–10] and the use of promoters [11–15]. In particular, bimetallic Co–Ni have been proven to offer superior performance for hydrocarbon reforming in terms of activity and stability compared to monometallic and other Ni-containing bimetallic combinations [8–10]. Additionally, the promotion of Ni catalysts with Ce has resulted in better activity and coking resistance, with the improvements attributed to the oxygen-storage capacity of Ce [11–16]. This work has examined the effect of Ce-promotion on bimetallic Co–Ni catalysts supported on Al_2O_3, as well as investigation of the kinetics and mechanism of CH_4 dry reforming on Co–Ni/Al_2O_3 and Ce–Co–Ni/Al_2O_3 catalysts.

2. Experimental

γ-Alumina (Saint-Gobain Nopro, USA) was first crushed and sieved to 140–425 μm before pre-treatment at 1073 K for 6 h. 5Co–15Ni/80Al_2O_3 and 2.5Ce–5Co–15Ni/77.5Al_2O_3 were then prepared via sequential wetness impregnation of the metal nitrates (Sigma–Aldrich, Australia) in the order Ce (for the promoted catalyst), Co and Ni. Previous studies [17,18] in our group have shown that Ce-promotion of the Co–Ni catalyst attained optimal dry reforming activity and reduced carbon deposition at Ce content greater than 1.5 wt%. Thus a Ce loading of 2.5 wt% was used to ensure optimal performance in the present investigation. Each impregnation step was followed by 3 h of stirring at ambient conditions, with subsequent drying for 24 h in an oven at 393 K. The resulting dried catalysts were calcined in air at heating rate of 5 K min^{-1} and held at 1073 K for 5 h. The calcined catalysts were then crushed and sieved to 140–250 μm before in situ activation with H_2 and subsequent reaction.

Multipoint BET surface area and pore volume and pore size measurements were obtained from N_2 adsorption at 77 K on a Quantachrome Autosorb-1 unit. Pulse H_2 chemisorption, CO_2-temperature-programmed desorption (TPD) and NH_3-TPD were performed on a Micromeritics Autochem 2910. Thermogravimetric analyses (calcination (TPC), reduction (TPR) and reduction–oxidation (TPR–TPO)) were performed in a ThermoCahn

☆ Student Award Paper.

* Corresponding author. Tel.: +61 2 9385 5268; fax: +61 2 9385 5966.
E-mail address: a.adesina@unsw.edu.au (A.A. Adesina).

0920-5861/$ – see front matter © 2010 Elsevier B.V. All rights reserved.
doi:10.1016/j.cattod.2010.10.092

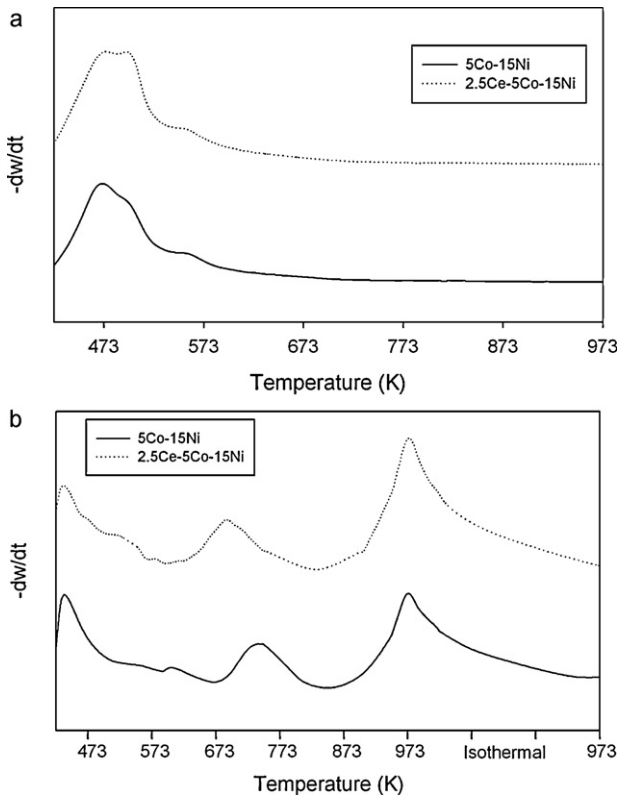

Fig. 1. Derivative weight profiles during (a) calcination and (b) reduction.

TherMax 200 system to study phase change and carbon gasification. Reaction products from TPR–TPO were qualitatively detected by a Pfeiffer Thermostar quadrupole mass spectrometer unit. All thermogravimetric experiments were carried out with the relevant gas flow rate of 55 mL min^{-1} (air for oxidation, 50%H_2/Ar for reduction) at a heating rate of 5 K min^{-1} and holding temperature of 973 K. The total carbon content of used catalysts (after a 4-h reaction run) was determined using a Shimadzu TOC Analyzer 5000A coupled to a solid sample module SSM-5000A.

Reaction runs were conducted on a computer-controlled experimental rig consisting of a gas manifold station, a stainless steel fixed-bed reactor (o.d. = 6.25 mm and i.d. = 4.57 mm) packed with 0.1 g of catalyst, and a TCD-equipped Shimadzu GC-17A gas chromatograph fitted with an Alltech CTR-1 column. Gas flow rates were regulated by Brooks Smart mass flow controllers. Prior to the reaction, the calcined catalyst was reduced in situ in 50 mL min^{-1} of 50%H_2/N_2 mixture at temperature ramp of 5 K min^{-1}, and held at 1063 K for 2 h. Following activation of the catalyst, the reactor was cooled under a blanket of N_2 to the reaction temperature. Gas hourly space velocity of 20,000 h^{-1} and catalyst particles limited to the size range 140–250 μm were used to minimise transport-disguised kinetics during data analysis. Runs were conducted over the temperature range 923–1023 K, with constant total pressure of 110 kPa. N_2 was employed as the diluent gas and tie-component for material balance purposes.

3. Results and discussion

3.1. Catalyst characterisation

The derivative weight profiles of the 2 catalysts during calcination are shown in Fig. 1(a). The main peak at about 473 K corresponds to the decomposition of the cobalt and nickel nitrates to their respective oxides, with the broad shoulder at 560 K indicating the formation of metal aluminates ($NiAl_2O_4$ and $CoAl_2O_4$). H_2-TPR profile of 5Co–15Ni (cf. Fig. 1(b)) implicates the reduction of Co_3O_4 and NiO to CoO and Ni respectively at 435 K, $NiCo_2O_4$ to Ni and CoO at 600 K, and CoO to Co at 740 K. The last peak at 973 K represents the reduction of the metal aluminates. Ce-doping did not appear to affect the calcination phase change profiles. However, reduction peaks for the doped catalysts were shifted to lower temperatures (by about 50 K). This observation has also been reported by Natesakhawat et al. [19] and Gallego et al. [16], and suggests that Ce-promotion increased ease of catalyst reduction.

Table 1
N_2 physisorption and H_2 chemisorption results.

	5Co–15Ni	2.5Ce–5Co–15Ni
BET area ($m^2\ g^{-1}$)	110.8 ± 1.1	110.7 ± 1.1
Pore volume ($cm^3\ g^{-1}$)	0.496 ± 0.005	0.454 ± 0.005
Average pore diameter (nm)	17.9 ± 0.2	16.4 ± 0.2
Metal dispersion (%)	0.580 ± 0.012	0.653 ± 0.013
Metal surface area ($m^2\ g_{cat}^{-1}$)	0.776 ± 0.016	0.874 ± 0.017
Active particle size (nm)	174 ± 3	154 ± 3

Table 1 summarises the N_2 physisorption and H_2 chemisorption data for the catalysts. The H_2 chemisorption results (metal dispersion, metal surface area and active particle size) were consistent with the high metal loading (20 wt%) used. While the BET surface area, pore volume and average pore diameter of both catalysts were similar, the Ce-promoted catalysts displayed higher metal dispersion and metal surface area along with smaller active particle size. The improved metal dispersion in Ce-containing catalysts has been attributed to strong metal-support interaction that occurs in CeO_2-supported or promoted catalysts [14,15]. NH_3- and CO_2-TPD results are displayed in Table 2. For both catalysts, NH_3-TPD and CO_2-TPD were characterised by 2 and 3 distinct peaks respectively. The first NH_3-TPD peak may be attributed to a weak Lewis acid site, while the second peak represents a strong Lewis acid site instead of a Brønsted site, since the latter typically exhibits ΔH_d greater than 125 kJ mol^{-1} [20]. Similarly, the CO_2-TPD indicates the presence of weak, intermediate and strong basic sites. In addition to the greater basic site strength (from higher in 2.5Ce–5Co–15Ni), Ce-promotion resulted in a lower acid-to-basic site ratio in the promoted catalyst, suggesting that doping with Ce increases the basicity of the catalyst.

3.2. Catalyst activity

Fig. 2(a)–(d) shows the CH_4, CO_2, H_2 and CO rates during CH_4 dry reforming at constant P_{CH_4} of 20 kPa and varying P_{CO_2}. While CH_4 consumption exhibited a weak dependency on P_{CO_2}, CO_2 consumption rose rapidly with CO_2 feed concentration. CO production showed similar behaviour to CO_2 consumption rate, however, the change in H_2 production rate with P_{CO_2} was insignificant, and seem

Table 2
Acidic and basic properties of the catalysts.

		5Co–15Ni	2.5Ce–5Co–15Ni
$\Delta H_{d,NH_3}$ (kJ mol^{-1})	I	43.3 ± 0.4	37.5 ± 0.8
	II	71.0 ± 0.7	71.6 ± 2.9
Acid site concentration (μmol m^{-2})	I	1.08 ± 0.02	1.13 ± 0.02
	II	2.89 ± 0.06	2.24 ± 0.04
	Total	3.97 ± 0.08	3.37 ± 0.06
$\Delta H_{d,CO_2}$ (kJ mol^{-1})	I	51.3 ± 2.6	68.5 ± 3.4
	II	68.0 ± 0.7	75.2 ± 0.8
	III	73.4 ± 0.7	86.7 ± 0.9
Basic site concentration (μmol m^{-2})	I	0.202 ± 0.004	0.242 ± 0.005
	II	0.209 ± 0.004	0.282 ± 0.006
	III	1.03 ± 0.02	0.98 ± 0.02
	Total	1.44 ± 0.03	1.50 ± 0.03
Acid-to-basic site ratio		2.75 ± 0.08	2.24 ± 0.07

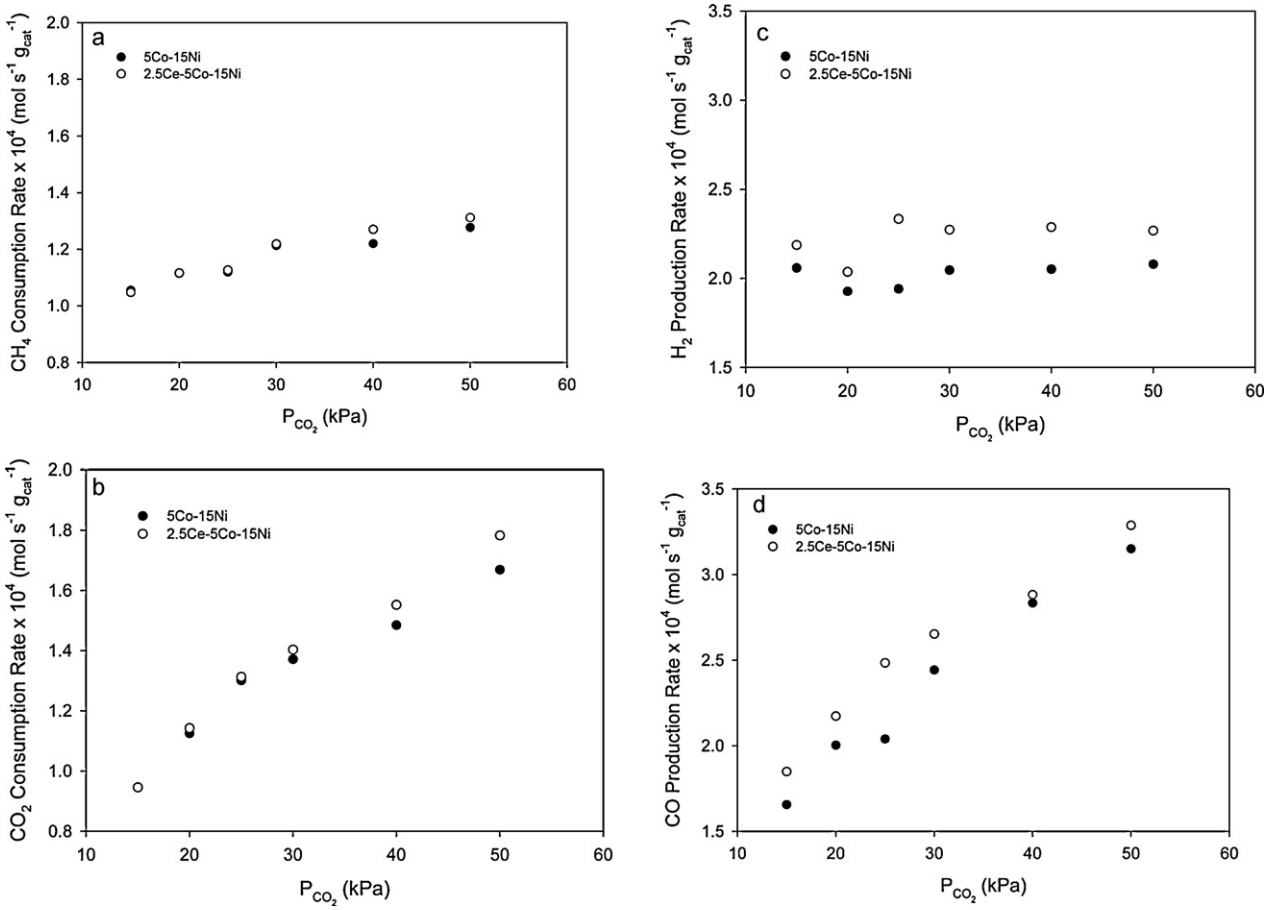

Fig. 2. (a) CH_4 consumption, (b) CO_2 consumption, (c) H_2 production and (d) CO production rates during CH_4 dry reforming at $P_{CH_4} = 20$ kPa and $T = 973$ K.

to plateau at $P_{CO_2} > 30$ kPa. H_2 was probably first produced via CH_4 dehydrogenation into carbonaceous C_xH_{1-x} [21]:

$$xCH_4 \rightarrow C_xH_{1-x} + \left(\frac{5x-1}{2}\right) H_2 \quad (1)$$

Subsequent interaction between CO_2 and the carbonaceous deposit yielded:

$$C_xH_{1-x} + xCO_2 \rightarrow 2xCO + \left(\frac{1-x}{2}\right) H_2 \quad (2)$$

Under excess feed CO_2 feed concentration, any additional H_2 produced may be readily converted to CO and water via the reverse water–gas shift reaction:

$$CO_2 + H_2 \rightarrow CO + H_2O \quad (3)$$

Comparison of the rate data between the two catalysts showed that CH_4 and CO_2 consumption rates were not affected significantly by Ce-promotion. However, H_2 and CO production rates seemed to increase in the Ce-promoted catalyst. Indeed, the promotional effect of the ceria may be attributed to its high oxygen storage capacity [22], in which Ce is able to exist to exist in multiple oxidation states while participating in redox reactions with surface carbon. Other investigations have also attributed improved catalyst activity, conversion and stability in hydrocarbon reforming to the redox properties of CeO_2 as well as the high mobility of lattice oxygen [14,15,19,23]. In particular, the redox steps involve the reduction of CeO_2 by unreacted C_xH_{1-x} to CeO_{2-x}, before re-oxidation back to CeO_2 by CO_2, viz;

$$CeO_2 + C_xH_{1-x} \leftrightarrow CeO_{2-x} + xCO + \left(\frac{1-x}{2}\right) H_2 \quad (4)$$

$$CeO_{2-x} + xCO_2 \leftrightarrow CeO_2 + xCO \quad (5)$$

3.3. Carbon deposition

Analysis of used catalysts for total carbon content demonstrated that Ce-promotion of bimetallic Co–Ni catalyst inhibited carbon deposition significantly, as shown in Fig. 3. The improvement in anti-coking characteristics of the catalyst may be attributed to the occurrence of redox reactions (Eqs. (4) and (5)) in the Ce-promoted catalyst. Additionally, the particle size required for carbon formation is larger than that required for CH_4 reforming [24]. Therefore, the improved metal dispersion and smaller active particle size of the Ce-promoted catalyst is likely to have played a part in reducing carbon deposition during CH_4 dry reforming. Based on data obtained over various feed compositions and temperatures, the global kinetics for carbon deposition may be expressed as:

$$r_{\text{carbon deposition}} = k_{dep} \exp\left(\frac{-E_{a,dep}}{RT}\right) P_{CH_4}^{a} P_{CO_2}^{b} \quad \text{for} \quad P_{CH_4} \le P_{CO_2} \le 1.5P_{CH_4} \quad (6)$$

The parameters of the model are displayed in Table 3, from whence it is apparent that activation energy values for both catalysts are negative in the range of temperatures studied. In particular, the kinetic expression (cf. Eq. (6)) applies only in cases when feed CO_2:CH_4 is greater than 1 but less than 1.5. Under CO_2-deficient conditions, carbon deposition increased with temperature as seen in Fig. 3. This phenomenon may be explained by examining the change in Gibbs energy for CH_4 dehydrogenation and carbon gasification by CO_2. While ΔG is negative for CH_4 dehydrogenation at our working temperatures (923–1023 K), ΔG for the CO_2 gasification reaction becomes negative only above 970 K. This suggest that

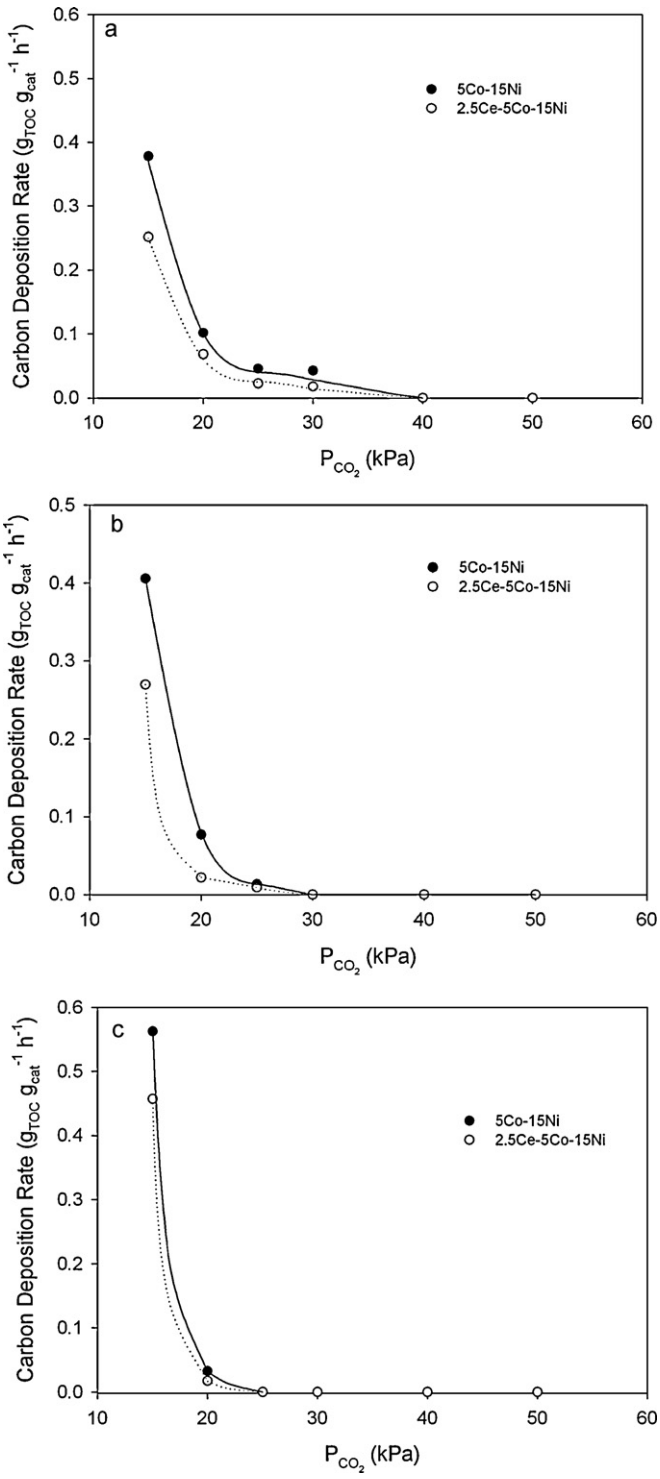

Fig. 3. Comparison of carbon deposition rate at between 2.5Ce–5Co–15Ni and 5Co–15Ni catalysts at varying P_{CO_2} at constant P_{CH_4} = 20 kPa, for (a) T = 923 K, (b) T = 973 K and (c) T = 1023 K.

Table 3
Parameter estimates for Eq. (6).

Parameter	5Co–15Ni	2.5Ce–5Co–15Ni
$k_{dep} \times 10^9$	7.27 ± 0.09	0.198 ± 0.004
$E_{a,\,dep}$ (kJ mol^{-1})	−92 ± 1.11	−107 ± 2.27
a	4.36 ± 0.05	5.54 ± 0.12
b	−2.75 ± 0.03	−3.65 ± 0.08

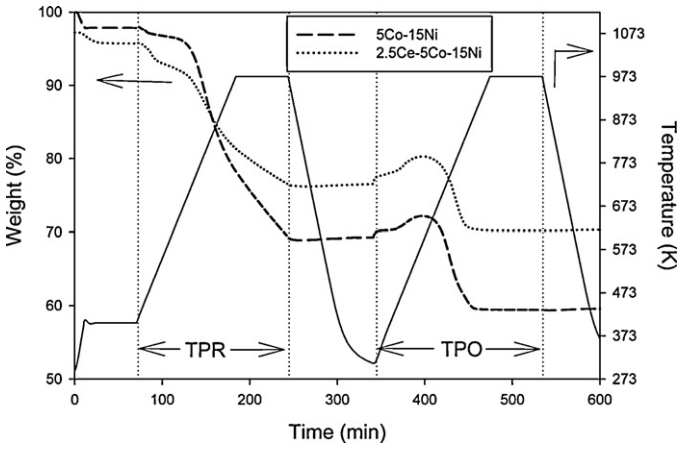

Fig. 4. Weight change profile during TPR–TPO for used catalysts after 4 h of stoichiometric dry reforming.

in the absence of CO_2, increased CH_4 dehydrogenation would lead to higher carbon deposition at higher temperatures; in the presence of sufficient amounts of CO_2 at high temperatures, carbon produced will be gasified by CO_2, leading to lower carbon deposition on the catalyst. At CO_2:CH_4 greater than 1.5, excess CO_2 results in gasification of all carbon deposits, resulting in undetectable quantities of carbon during post-reaction analysis.

TPR–TPO of the used catalysts showed similar profiles for both catalysts. The typical TPR–TPO profile is displayed in Fig. 4, which shows the weight change of the used 5Co–15Ni and 2.5Ce–5Co–15Ni catalysts after 4 h of stoichiometric CH_4 dry reforming at 923 K. Clearly, the weight change of the used Ce-promoted catalyst is lower since it contained smaller amount of deposited carbon. The reaction products during TPR–TPO were detected by mass spectrometry as shown in Fig. 5. Reaction of surface carbonaceous species with H_2 during the TPR stage produced only CH_4, with no detectable C_{2+} products. The CH_4 production profile was characterised by a distinct peak followed by a gentle decline for the rest of the TPR stage, while the CO_2 production profile showed a clear peak, after which no additional CO_2 was produced – indicating that there was no surface carbon left on the catalyst after the TPO regime. These results suggest that there are two types of carbonaceous pools present on the catalyst – one which is readily gasified by both H_2 and O_2, and another which is only reactive with O_2. Based on the nature of carbon reactivity, the more reactive carbon species was identified as C_α (atomic carbon),

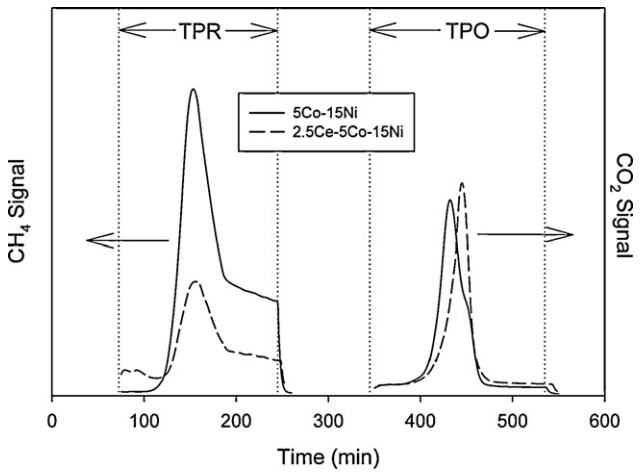

Fig. 5. Reaction products during TPR–TPO as detected by mass spectrometry.

while C_β (dehydropolymerised carbon species) was only able to react easily with O_2 [25]. Comparison of the two catalysts showed that while used Ce-promoted catalyst produced lower amount of CH_4 during TPR, similar quantities of CO_2 were produced during the TPO stage. It would therefore seem that while Ce-promotion of catalysts reduced carbon deposition significantly through the redox mechanism, much of the carbon that is removed is C_α. Based on this observation, it seems that C_β does not participate readily in the redox reactions with ceria.

3.4. Kinetic model

Many mechanisms regarding the CH_4 dry reforming reaction have been proposed in past investigations by various authors using different techniques. Osaki et al. [26,27] employed pulse surface reaction analysis to study CH_4 dry reforming on various supported Ni catalysts, and found that adsorbed CH_y is produced via sequential elimination of hydrogen atoms (where y varied between 1 and 2.7 in their study), eventually leading to surface carbon. Stevens and Chuang [28], using combined in situ infrared (IR) spectroscopic and mass spectrometric study, suggested that CH_4 was first decomposed into CH_y species and H_2 over Rh/Al_2O_3. Erdöhelyi et al. [29,30], while studying CH_4 and CO_2 activation using IR methods, found that CO_2 adsorption is dissociative in nature due to the presence of adsorbed CO-band signals. On the other hand, Bradford and Albert Vannice [31] suggested that CO_2 adsorption is non-dissociative due to the existence of bands representing carbonates during in situ DRIFTS experiments. Based on our NH_3- and CO_2-TPD data, we propose the following sequence of elementary steps describing the CH_4 dry reforming reaction:

$$CH_4 + 2X_1 \leftrightarrow CH_3\text{-}X_1 + H\text{-}X_1 \quad (7a)$$

$$CH_3\text{-}X_1 + X_1 \leftrightarrow CH_y\text{-}X_1 + H\text{-}X_1 \quad 1 \le y \le 3$$

$$\vdots \quad (7b)$$

$$CH\text{-}X_1 + X_1 \leftrightarrow C\text{-}X_1 + H\text{-}X_1$$

$$CO_2 + 2X_2 \leftrightarrow CO\text{-}X_2 + O\text{-}X_2 \quad (7c)$$

$$C\text{-}X_1 + O\text{-}X_2 \rightarrow CO\text{-}X_2 + X_1 \quad \text{r.d.s.} \quad (7d)$$

$$2H\text{-}X_1 \leftrightarrow H_2 + 2X_1 \quad (7e)$$

$$CO\text{-}X_2 \leftrightarrow CO + X_2 \quad (7f)$$

$$H\text{-}X_1 + O\text{-}X_2 \rightarrow OH\text{-}X_2 + X_1 \quad (7g)$$

$$H\text{-}X_1 + OH\text{-}X_2 \leftrightarrow H_2O + X_1 + X_2 \quad (7h)$$

where X_1 and X_2 are the two different sites. Based on this dual-site mechanism, with Eq. (7d) as the rate-determining step, a Langmuir–Hinshelwood kinetic model was derived as:

$$-r_{CH_4} = \frac{k_{rxn}\sqrt{P_{CH_4}}\sqrt{P_{CO_2}}}{(1+\sqrt{K_{CH_4}P_{CH_4}})(1+\sqrt{K_{CO_2}P_{CO_2}})} \quad (8)$$

where:

$$k_{rxn} = A\exp\left(\frac{-E_a}{RT}\right) \quad (9a)$$

$$K_{CH_4} = \exp\left(\frac{\Delta S_{ads,CH_4}}{R}\right)\exp\left(\frac{-\Delta H_{ads,CH_4}}{RT}\right) \quad (9b)$$

$$K_{CO_2} = \exp\left(\frac{\Delta S_{ads,CO_2}}{R}\right)\exp\left(\frac{-\Delta H_{ads,CO_2}}{RT}\right) \quad (9c)$$

The parameter estimates for Eqs. (9a)–(9c) for both promoted and unpromoted Co–Ni catalysts are listed in Table 4. The adequacy of the model may be seen from the parity plots in Fig. 6(a) and (b) which shows a good fit of the model to the experimental data.

Table 4
Parameter estimates for Eqs. (9a)–(9c).

Parameter	5Co–15Ni	2.5Ce–5Co–15Ni
$A \times 10^3$ (mol g_{cat}^{-1} s^{-1} kPa^{-1})	12.32 ± 0.24	9.54 ± 0.17
E_a (kJ mol^{-1})	56.40 ± 1.14	54.52 ± 0.96
$\Delta S_{ads,CH_4}$ (J mol^{-1} K^{-1})	−229.13 ± 4.63	−79.11 ± 1.40
$\Delta H_{ads,CH_4}$ (kJ mol^{-1})	98.31 ± 1.99	248.15 ± 4.38
$\Delta S_{ads,CO_2}$ (J mol^{-1} K^{-1})	−93.04 ± 1.88	−133.04 ± 2.35
$\Delta H_{ads,CO_2}$ (kJ mol^{-1})	−61.92 ± 1.25	−99.41 ± 1.76

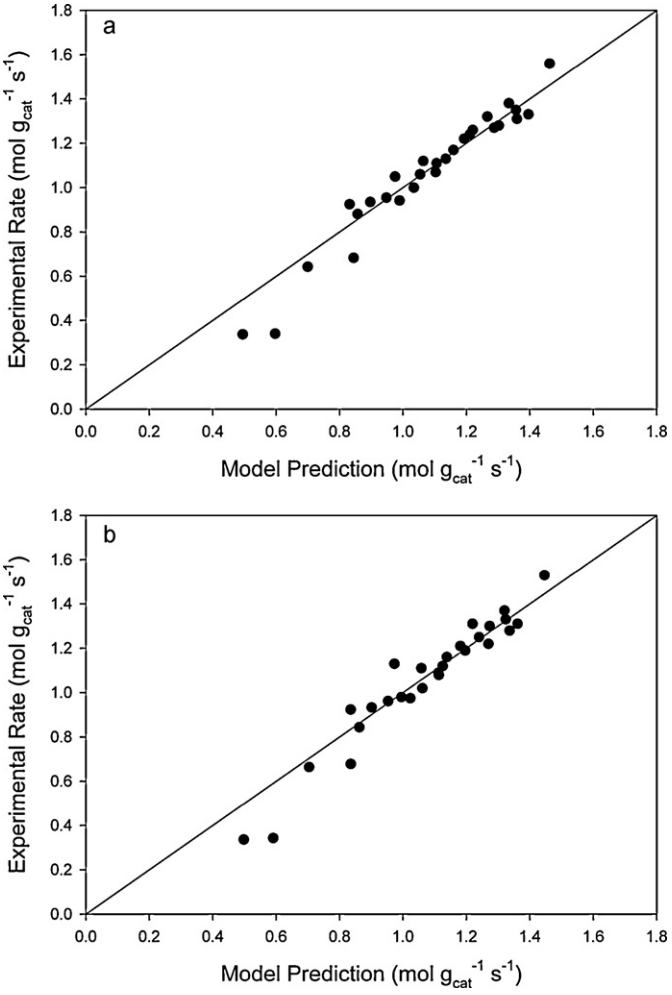

Fig. 6. Parity plots comparing experimental rates and predicted rates for (a) 5Co–15Ni and (b) 2.5Ce–5Co–15Ni.

4. Conclusions

This study has examined the performance of both Ce-promoted and unpromoted bimetallic Co–Ni catalysts supported on alumina. The most apparent effect of Ce-promotion was in reduction of carbon deposition due to participation of cerium oxides in redox reactions with carbonaceous deposits. For both catalysts, TPR–TPO revealed the presence of at least two types of carbonaceous deposits, the reactive C_α and non-reactive C_β. Analysis of mass spectrometry results during TPR–TPO suggested that C_β does not participate in the redox reactions with Ce-promoter. A dual-site Langmuir–Hinshelwood mechanism was proposed based on our experimental data.

Acknowledgements

The authors appreciate financial support from the Australian Research Council. SYF and CKC are recipients of the Australian Postgraduate Award and University International Postgraduate Research Award scholarships respectively.

References

[1] Y.H. Hu, E. Ruckenstein, Adv. Catal. 48 (2004) 297.
[2] A.T. Ashcroft, A.K. Cheetham, M.L.H. Green, P.D.F. Vernon, Nature 352 (1991) 255.
[3] M. García-Diéguez, I.S. Piesta, M.C. Herrera, M.A. Larrubia, L.J. Alemany, J. Catal. 270 (2010) 136.
[4] Z. Hou, P. Chen, H. Fang, X. Zheng, T. Yashima, Int. J. Hydrogen Energy 31 (2006) 555.
[5] J.R. Rostrup-Nielsen, J.-H. Bak Hansen, J. Catal. 144 (1993) 38.
[6] L.B. Råberg, M.B. Jensen, U. Olsbye, C. Daniel, S. Haag, C. Mirodatos, A.O. Sjåstad, J. Catal. 249 (2007) 250.
[7] E. Ruckenstein, Y.H. Hu, J. Catal. 162 (1996) 230.
[8] K. Opoku-Gyamfi, K. Tafreshi, A.A. Adesina, React. Kinet. Catal. Lett. 64 (1998) 229.
[9] K. Takanabe, K. Nagaoka, K. Nariai, K. Aika, J. Catal. 232 (2005) 268.
[10] J. Zhang, H. Wang, A.K. Dalai, J. Catal. 249 (2007) 300.
[11] Z. Cheng, Q. Wu, J. Li, Q. Zhu, Catal. Today 30 (1996) 147.
[12] T.-J. Huang, H.-J. Lin, T.-C. Yu, Catal. Lett. 105 (2005) 239.
[13] R. Martinez, E. Romero, C. Guimon, R. Bilbao, Appl. Catal. A 274 (2004) 139.
[14] A. Nandini, K.K. Pant, S.C. Dhingra, Appl. Catal. A 290 (2005) 166.
[15] S. Wang, G.Q. Lu, Appl. Catal. B 19 (1998) 267.
[16] G.S. Gallego, J.G. Marín, C. Batiot-Dupeyrat, J. Barrault, F. Mondragón, Appl. Catal. A 369 (2009) 97.
[17] F.M. Althenayan, S.Y. Foo, E.M. Kennedy, B.Z. Dlugogorski, A.A. Adesina, Chem. Eng. Sci. 65 (2010) 66.
[18] F.M. Althenayan, C.B. Dave, A.A. Adesina, 6th International Conference on Environmental Catalysis, Beijing, China, 12–15 September, 2010.
[19] S. Natesakhawat, O. Oktar, U.S. Ozkan, J. Mol. Catal. A: Chem. 241 (2005) 133.
[20] G. Yaluris, R.B. Larson, J.M. Kobe, M.R. González, K.B. Fogash, J.A. Dumesic, J. Catal. 158 (1996) 336.
[21] S.Y. Foo, C.K. Cheng, T.-H. Nguyen, A.A. Adesina, Ind. Eng. Chem. Res. 49 (2010) 10450.
[22] K. Otsuka, T. Ushiyama, I. Yamanaka, Chem. Lett. 22 (1993) 1517.
[23] N. Laosiripojana, W. Sangtongkitcharoen, S. Assabumrungrat, Fuel 85 (2006) 323.
[24] J.R. Rostrup-Nielsen, H.B. Calvin, B.B. John, Stud. Surf. Sci. Catal. 68 (1991) 85.
[25] K.M. Hardiman, C.G. Cooper, A.A. Adesina, R. Lange, Chem. Eng. Sci. 61 (2006) 2565.
[26] T. Osaki, H. Masuda, T. Mori, Catal. Lett. 29 (1994) 33.
[27] T. Osaki, T. Horiuchi, K. Suzuki, T. Mori, J. Chem. Soc. Faraday Trans. 92 (1996) 1627.
[28] R.B.J. Stevens, S.S.C. Chuang, J. Phys. Chem. B 108 (2004) 696.
[29] A. Erdöhelyi, J. Cserényi, F. Solymosi, J. Catal. 141 (1993) 287.
[30] A. Erdöhelyi, J. Cserényi, E. Papp, F. Solymosi, Appl. Catal. A 108 (1994) 205.
[31] M.C.J. Bradford, M. Albert Vannice, Catal. Today 50 (1999) 87.